

## Ni Microspheres as Electrocatalysts for Ethanol Oxidation in an Alkaline Medium

A. Altamirano-Gutiérrez, G.E. Martínez-Tapia, L.C. Ordóñez\*

Unidad de Energía Renovable, Centro de Investigación Científica de Yucatán A. C., Parque Científico Tecnológico de Yucatán, Carretera Sierra Papacal-Chuburna Puerto Km 5, Sierra Pacacal, Yucatán, México. C. P. 97302. Tel.: +52 (999) 9300760, Ext. 1205.

\*E-mail: [icol@cicy.mx](mailto:icol@cicy.mx)

Received: 30 November 2017 / Accepted: 29 January 2018 / Published: 10 April 2018

---

We report the synthesis of nickel microspheres and their structural and electrochemical characterization. The materials were prepared by the microemulsion technique from  $\text{NiSO}_4 \cdot 6\text{H}_2\text{O}$  and  $\text{NaOH}$ , and using  $\text{NaH}_2\text{PO}_2 \cdot \text{H}_2\text{O}$  as a reducing agent. Sodium dodecyl sulfate (SDS) was used as a surfactant. The following ternary formulations were used for their synthesis: N1 (90%  $\text{H}_2\text{O}$ -7.5% SDS-2.5% Pentanol), N2 (92.5%  $\text{H}_2\text{O}$ -5% SDS-2.5% Pentanol), N3 (95%  $\text{H}_2\text{O}$ -3.75% SDS-1.25% Pentanol) and N4 (99%  $\text{H}_2\text{O}$ -0.75% SDS-0.25% Pentanol). The catalysts were characterized by scanning electron microscopy (SEM) and X-ray diffraction (XRD). The catalytic activity for ethanol oxidation in an alkaline medium was evaluated by cyclic voltammetry (CV) and electrochemical impedance spectroscopy (EIS). The average diameters of the nickel microspheres ranged from 0.375 to 1.476  $\mu\text{m}$ . On subjecting the materials to heat treatment in a nitrogen atmosphere at 300 °C for 4 h, mixtures of polycrystalline Ni and nickel phosphide ( $\text{Ni}_3\text{P}$ ) were obtained. The best performance for the ethanol oxidation reaction (EOR) in an alkaline medium was recorded with non-heat-treated nickel microspheres, presenting a maximum peak potential at approximately 0.7 V vs.  $\text{Hg}/\text{HgO}$  with normalized currents between 10.774 and 18.198  $\text{mA}(\text{mgcat})^{-1}$ . These results indicate that nickel microspheres are potential candidates for use as anodes in alkaline direct alcohol fuel cells (A-DAFCs).

---

**Keywords:** Nickel microspheres, microemulsion synthesis, electrocatalysts, anode, alkaline direct alcohol fuel cells.

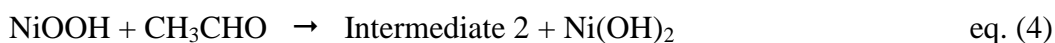
### 1. INTRODUCTION

Fuel cells are widely considered to be sustainable and efficient energy conversion devices. They are undergoing rapid development for mobile applications, particularly for the transport sector. Various fuels such as hydrogen, methanol and ethanol, have been used in fuel cells with certain

advantages and disadvantages [1]. However, ethanol offers greater sustainability for use in direct alcohol fuel cells (DAFCs) [2-4]. Catalysis for the oxidation of alcohols has generally been performed with precious metals, such as Pt, Au, Pd, Ag, Ru and Rh [4]. On the other hand, transition metal catalysts, such as Ni, Cu, and Co, have been found to be more economical for carrying out the reaction under alkaline conditions. Nickel has been used as an electrocatalyst for both anodic and cathodic reactions in organic synthesis, water electrolysis [5] and for the electro-oxidation of alcohols [6-8]. Van Effen and Evans studied ethanol oxidation with nickel in a KOH solution and identified that the reaction occurs with the formation of a higher valence nickel oxide which acts as an oxidizing agent [9, 10]. Taraszewska and Roslonek [11] found that a glassy carbon electrode modified by nickel hydroxide (GC/Ni(OH)<sub>2</sub>) was an effective catalyst for methanol oxidation. It has been reported that a Ni-zeolite/graphite material presented greater activity than Ni and Pt for the methanol oxidation reaction in an alkaline medium [12]. Mukherjee and collaborators [13] studied binary mixtures of Ni/Pt (1, 5, 10, 30, 60 and 120) in 1.0 M NaOH + 1.0 M CH<sub>3</sub>CH<sub>2</sub>OH and found that a catalyst containing a 1:1 atomic ratio of Pt to Ni showed the highest electrocatalytic activity for the ethanol oxidation reaction (EOR) in an alkaline medium, expressed as greater current density and poisoning tolerance. Wang and collaborators [14] synthesized Ni/Al<sub>2</sub>O<sub>3</sub> electrocatalysts using the solvent evaporation induced self-assembly method. This material presented a competitive ethanol electrooxidation activity in alkaline media attributed to an improved mass transfer explained by a homogeneous Ni particles distribution on the support surface and mesoporous textural properties.

A large amount of research has been carried out in synthesizing metal spheres by means of a removable template, such as an inorganic core (zinc, silica), surfactant micelles, polymer-micelle complexes and liquid drops [15, 16]. Liu and co-workers [17] manufactured nickel spheres using a surfactant micelle as a soft template. However, it is not easy to obtain a uniform nickel microsphere with the use of these methods. Nickel spheres can also be obtained via in situ redox reactions of Ni<sup>2+</sup> with H<sub>2</sub>PO<sub>2</sub><sup>-</sup> in an emulsion [18], from colloidal particles of Ni(OH)<sub>2</sub> [19], and via micellar media of Ni(DS)<sub>2</sub> (nickel dodecyl sulfate) [17]. Electroless plating methods [20, 21] are simple and suitable for nickel compounds and microspheres.

The ethanol oxidation mechanism at nickel electrodes in alkaline medium was proposed by Fleishmann and collaborators [22]. The proposed mechanism can be summarized as follows:



The conversion of ethanol to acetic acid was reported at 98% [22, 23]. Additionally, acetaldehyde (CH<sub>3</sub>CHO) [24, 25], CH<sub>3</sub>O and CO [26-28] have been reported as oxidation intermediates. The rate-determining step of the ethanol oxidation reaction at nickel electrodes is the oxidation of nickel hydroxide to higher valence oxides/oxyhydroxides [29].

In this work, we synthesized nickel-based electrocatalysts in the form of microspheres using nickel sulfate as the source in a microemulsion with different water-sodium dodecyl sulfate-pentanol ratios. Sodium hypophosphite was used as a reducing agent. The aim was to determine the catalytic performance for the ethanol electro-oxidation reaction in alkaline medium for these Ni materials, both fresh and after treatment at 300 °C in a nitrogen atmosphere.

## 2. EXPERIMENTAL

### 2.1. Preparation of the catalysts

Ni microspheres were prepared by the microemulsion synthesis method [30]. Four H<sub>2</sub>O-SDS-Pentanol ternary formulations were prepared with different ratios: N1) 90%-7.5%-2.5%, N2) 92.5%-5%-2.5%, N3) 95%-3.75%-1.25% and N4) 99%-0.75%-0.25%. Appropriate quantities of NiSO<sub>4</sub>·6H<sub>2</sub>O, NaOH, and NaH<sub>2</sub>PO<sub>2</sub>·H<sub>2</sub>O were used. The total volume was 60 mL, and the temperature was maintained at 80 °C for 10 minutes to achieve thermal homogenization in the micelles formation. The reaction mixture color changed from bright green to pastel green due to the formation of a fine Ni(OH)<sub>2</sub> gel. Following a period of agitation, rapid hydrogen gas evolution was generated accompanied by the precipitation of fine dark gray particles. The reaction mixture changed color from pastel green to dark gray. The reaction continued for 2 h. The precipitate was separated by centrifugation at 3,000 rpm for 10 minutes. It was washed several times with deionized water. The recovered product was filtered and subsequently washed consecutively with methanol and ethyl ether. Finally, the product was dried in a vacuum oven at 80 °C for 16 h. The Ni catalysts obtained were named according to the ternary formulation that was used. Two series of materials were prepared. The first consisted of the fresh materials and the second consisted of the materials subjected to heat treatment at 300 °C for 4 h in a nitrogen atmosphere. The heating rate was 10 °C min<sup>-1</sup>. Ni nanopowder from Sigma-Aldrich (577995) was evaluated as a reference catalyst.

### 2.2. Physical characterization of the electrocatalysts

The elemental chemical composition was obtained with an energy dispersive X-ray (EDX) microanalysis system in a Philips XL30 ESEM microscope. Morphological characterization was performed with a Jeol JSM-6360LV scanning electron microscope (SEM). X-ray diffraction (XRD) patterns were obtained with a Siemens D-5000 diffractometer (CuK $\alpha$  radiation,  $\lambda = 1.5405 \text{ \AA}$ ).

### 2.3. Preparation of the electrode

An ink was prepared by dispersing 2.0 mg of catalyst and 4.6 mg of Vulcan XC-72R carbon in 100  $\mu\text{L}$  of isopropanol plus 80  $\mu\text{L}$  of 5% Nafion® solution. These components were homogenized in an ultrasonic bath for 15 minutes. An aliquot of 2.0  $\mu\text{L}$  of the catalytic ink was deposited on a glassy carbon electrode (geometric area of 0.0701 cm<sup>2</sup>) that was left to dry at room temperature.

#### 2.4. Electrochemical characterization of the electrocatalysts

The electrochemical measurements were carried out at room temperature using a three-electrode electrochemical cell coupled to a potentiostat/galvanostat with a FRA module (Autolab, PGSTAT-302). A graphite rod was used as the counter electrode. A mercury/mercuric oxide electrode (Hg/HgO, 1.0 M NaOH) was used as a reference, and each of the synthesized materials were used as a working electrode. The supporting electrolyte was 1.0 M NaOH. Before each test, the supporting electrolyte or the working medium (1.0 M NaOH + 1.0 M CH<sub>3</sub>CH<sub>2</sub>OH) were saturated with nitrogen for 30 minutes. The cyclic voltammetry (CV) measurements were performed over a potential range of -1.0 to 0.8 V at a sweep rate of 50 mVs<sup>-1</sup>. With the supporting electrolyte, 30 cycles were performed and the final one was selected. The open-circuit potential (OCP) was measured at the start and end of the cycles. CV tests on the working medium were performed at a sweep rate of 10 mVs<sup>-1</sup>. Potentiostatic electrochemical impedance measurements were performed over a frequency range of 60 kHz to 0.1 Hz, with an AC amplitude of 10 mV throughout the frequency range at each of the DC potentials: 0.45, 0.50, 0.60 V vs. Hg/HgO.

### 3. RESULTS AND DISCUSSION

#### 3.1. Physicochemical characterization

The elemental analysis results obtained by EDX are shown in Table 1. The weight percentage of nickel ranges between 71 and 88%, while the percentage of phosphorus lies between 8 and 13%. The phosphorus present originates from the sodium hypophosphite salt that it was not eliminated with the washing performed with water, methanol and ethyl ether. On the other hand, a significant percentage of oxygen was observed, between 5 and 15%, and this is attributed to some materials absorbing moisture from the atmosphere. Maximovitch and Bronoel [31] reported that smooth nickel electrodes are very sensitive to the presence of molecular oxygen dissolved in a solution and identified its adsorption on their surface.

**Table 1.** Elemental composition of the prepared Ni catalysts: N1-N4, untreated fresh materials and materials heat treated in a nitrogen atmosphere at 300 °C for 4 h.

Catalyst	Untreated fresh materials			Heat treated materials		
	Ni (Wt. %)	P (Wt. %)	O (Wt. %)	Ni (Wt. %)	P (Wt. %)	O (Wt. %)
N1	88.86	8.73	2.41	86.72	8.27	5.01
N2	77.64	11.91	10.45	78.82	11.39	9.79
N3	73.18	13.09	13.73	71.96	11.90	16.14
N4	71.68	11.48	16.84	74.54	11.78	13.68

Figure 1 shows the SEM images of the non-heat-treated N1, N2, N3 and N4 nickel materials. All of the micrographs have a magnification of 10,000X. The microemulsion synthesis conditions

clearly have a significant influence on the morphology of the Ni particles. For samples N1 and N2, well-defined Ni microspheres with smooth surfaces were observed. The histograms obtained for the two samples present a monomodal behavior that, after being fitted to a normal curve, gives a diameter with average sizes of 0.825 and 0.530  $\mu\text{m}$ , respectively (Fig. 1a). The histogram for the N2 material is narrower than for the other three samples (Fig. 1b). For samples N3 and N4, a spherical Ni morphology was observed with average sizes of 0.951 and 0.997  $\mu\text{m}$ , respectively (Table 2). In particular, samples N3 and N4 are surrounded by smaller Ni particles with an irregular morphology. Meanwhile, N3 has few nickel spheres. Irregularly shaped particles are more abundant and its histogram does not fit a normal curve (Fig. 1c). The N4 material presents a normal trend in the size distribution of Ni microspheres (Fig. 1d).

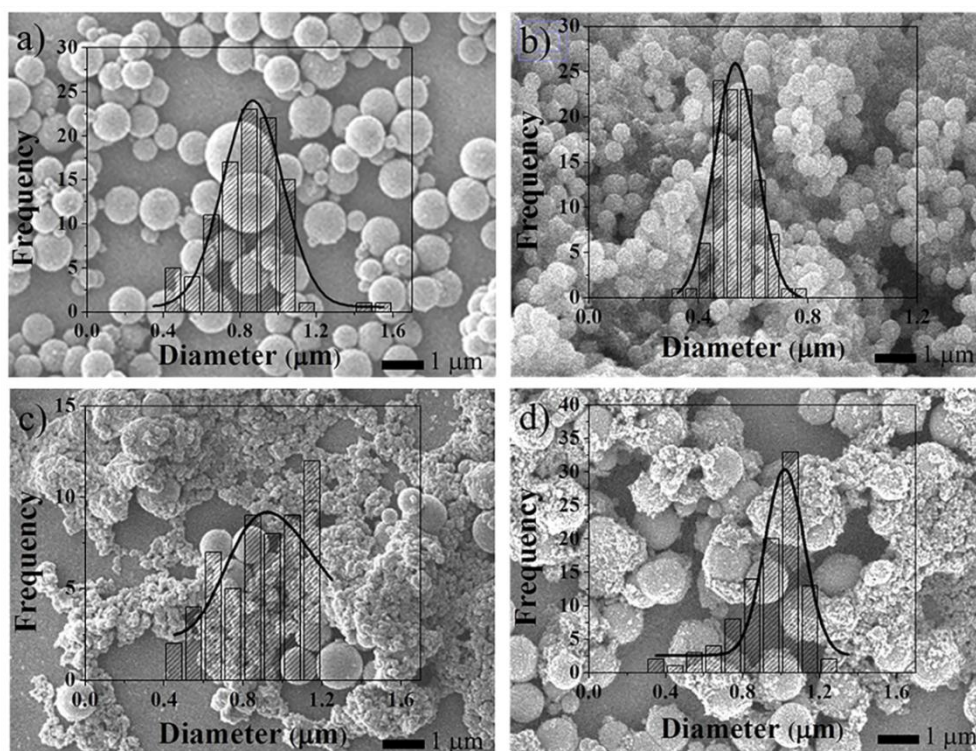
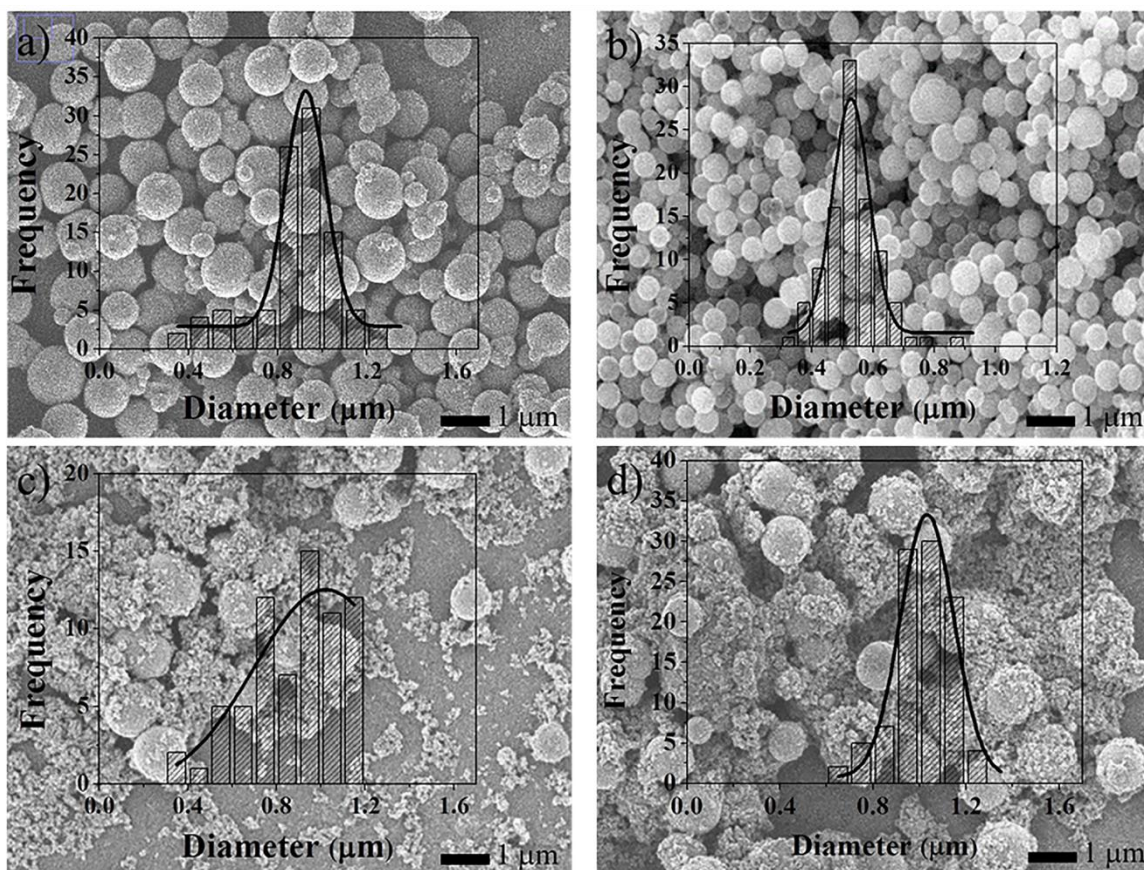


**Figure 1.** SEM micrographs of nickel microspheres synthesized by microemulsion: non-heat-treated N1, N2, N3 and N4 and their frequency histograms based on diameter a), b), c) and d) respectively.

**Table 2.** Average diameters of nickel microspheres obtained by SEM and crystal size measurements of Ni and Ni<sub>3</sub>P calculated by XRD analysis.

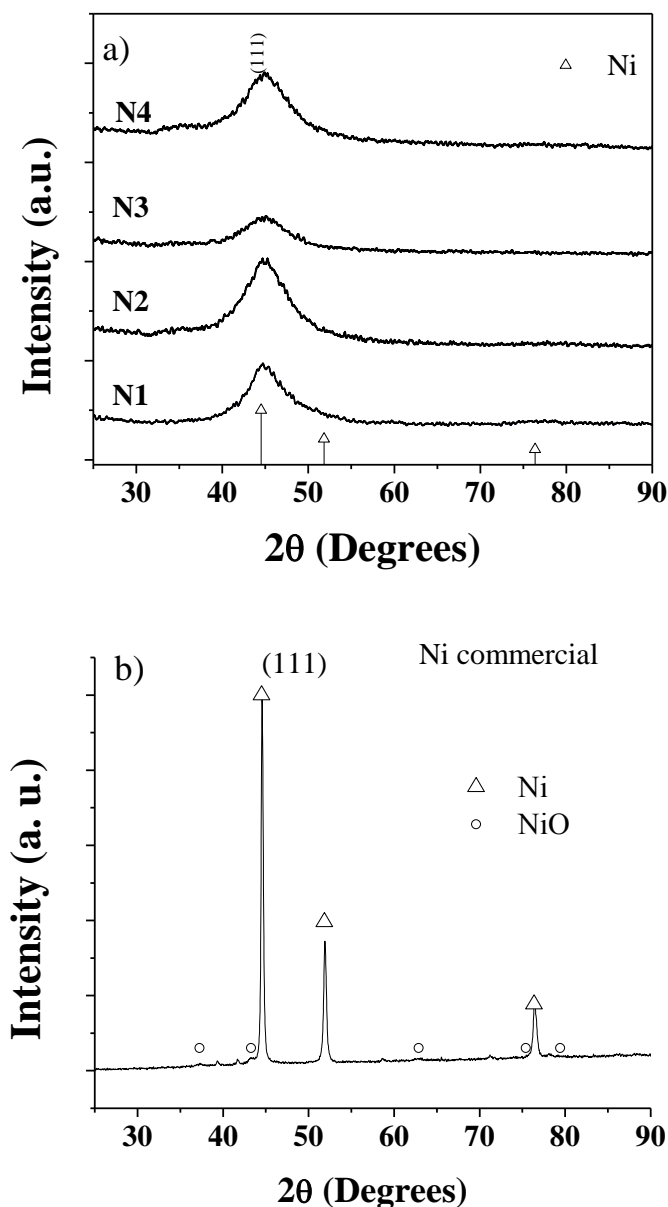
Catalyst	Untreated fresh materials		Heat treated materials	
	Microsphere diameter ( $\mu\text{m}$ )	Ni crystal size (nm)	Microsphere diameter ( $\mu\text{m}$ )	Ni <sub>3</sub> P crystal size (nm)
N1	$0.825 \pm 0.315$	2.1	$0.909 \pm 0.180$	20.8
N2	$0.530 \pm 0.155$	1.7	$0.524 \pm 0.118$	9.8
N3	$0.951 \pm 0.241$	1.5	$0.828 \pm 0.648$	13.9
N4	$0.997 \pm 0.205$	1.7	$1.05 \pm 0.230$	21.1
Commercial Ni	$0.473 \pm 0.016$	30.5	---	---

Figure 2 shows micrographs of the catalysts that were subjected to heat treatment in a nitrogen atmosphere at 300 °C for 4 h. In all cases, the nickel microspheres have an average diameter of approximately 1  $\mu\text{m}$ , except for N2, which was half a micrometer (Table 2). Similarly, for samples N1, N2 and N4, the distribution histograms follow the same monomodal trend as their untreated counterparts (Figs. 2a, 2b and 2d, respectively). Nevertheless, the standard deviation of N3 is the highest, with a value of 0.648 microns, as corroborated by its histogram (Fig. 2c), which does not follow a normal curve. The average diameters and their deviations are reported in Table 2.



**Figure 2.** SEM micrographs of nickel microspheres synthesized by microemulsion: N1, N2, N3 and N4 heat-treated in nitrogen atmosphere at 300 °C,  $t = 4$  h, and their distribution histograms based on diameters a), b), c) and d), respectively.

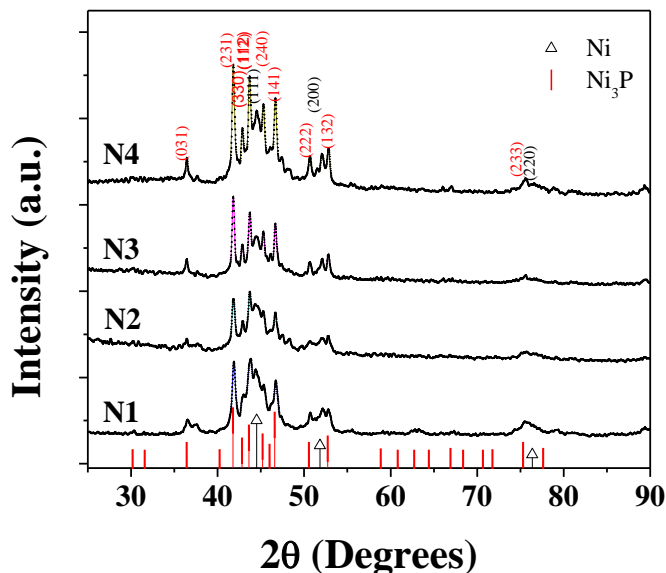
Figure 3 shows the X-ray diffractograms for the fresh, non-heat-treated N1, N2, N3, N4 samples and the commercial Ni sample. In the entire series, a wide diffraction peak can be seen located at  $44.5^\circ 2\theta$  corresponding to the (111) plane of metallic nickel (JCPDS, PDF 04-0850), with a crystalline face-centered cubic (fcc) structure. On the other hand, no diffraction line was observed related to the phosphorus present in the four samples; it is probably found in the interstices of the crystalline nickel lattice, or perhaps an amorphous nickel-phosphorus compound formed [20]. For the commercial Ni sample diffractions lines were observed corresponding to metallic nickel and diffractions peaks located at  $37.5$ ,  $43.3$ ,  $62.9$ ,  $75.5$ , and  $79.5^\circ 2\theta$  corresponding to the (111), (220), (311), and (222) planes of the fcc structure of NiO (JCPDS, PDF 04-0835).



**Figure 3.** X-ray diffraction patterns of nickel microspheres: a) non-heat-treated N1, N2, N3, and N4, b) commercial Ni.

Figure 4 shows the XRD patterns of the nickel microspheres treated for 4 h at 300 °C in nitrogen atmosphere. Diffraction peaks were observed in similar positions compared to the face-centered cubic (fcc) phase of Ni (JCPDS, PDF 04-0850), corresponding to the (111), (200) and (220) planes, located at 44.5°, 51.8° and 76.3°, respectively. Additionally, in all of our samples, reflections were observed in positions corresponding to the body-centered tetragonal phase of Ni<sub>3</sub>P (JCPDS, PDF 34-0501), corresponding to the (031), (231), (330), (112), (240), (141), (222), (132) and (233) planes located at 36.4°, 41.7°, 42.8°, 43.6°, 45.2°, 46.6°, 50.5°, 52.7° and 75.3°, respectively. The Ni<sub>3</sub>P compound was formed upon subjecting the samples to 300 °C in nitrogen. This was similar to the results of Bernardi and collaborators [32], who obtained nickel phosphide (Ni<sub>3</sub>P) by means of heat

treatment at 350 °C for 3 h. The Ni<sub>3</sub>P diffraction peaks presented greater intensity than the nickel peaks, which is attributed to a greater degree of crystallinity.

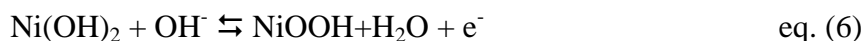


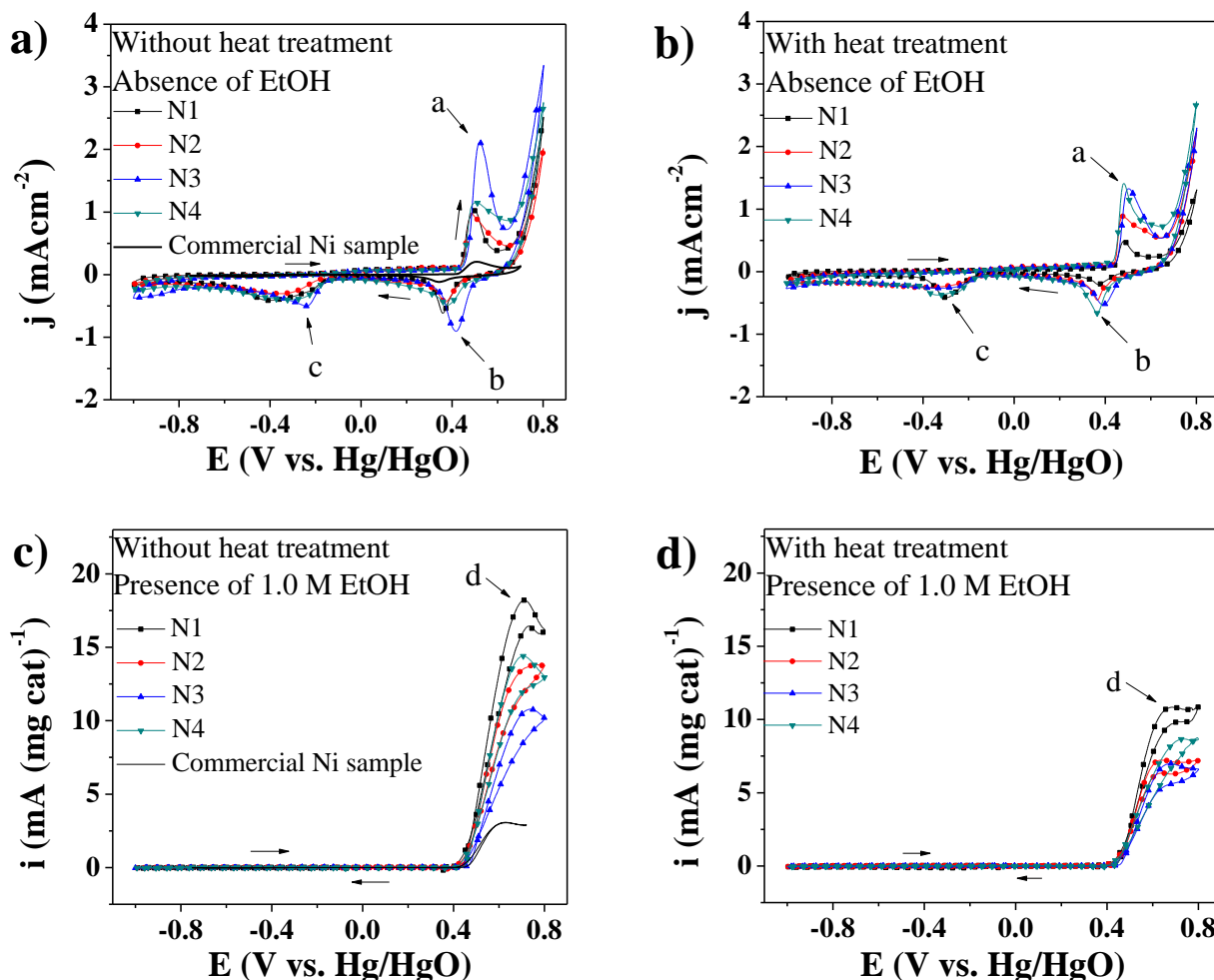
**Figure 4.** X-ray diffraction patterns of nickel microspheres: N1, N2, N3 and N4, treated in a nitrogen atmosphere at 300 °C for 4 h.

Table 2 shows the crystal size of the nickel microspheres calculated via the Scherrer equation using the full-width at half-maximum (FWHM) of the most intense diffraction peaks [33]. For the fresh samples, metallic nickel crystallites were obtained with an average size of between 1.5 and 2.1 nm. Following the heat treatment at 300 °C in nitrogen, mixtures of Ni and Ni<sub>3</sub>P were obtained and the diffraction peaks of polycrystalline nickel overlapped those of the nickel phosphide phases (Fig. 4), meaning it was not possible to determine the Ni crystal size. However, the average Ni<sub>3</sub>P crystal size was found to be between 9 and 21 nm. The commercial Ni sample showed a metallic nickel crystallite size of 30.5 nm

### 3.2. Electrochemical characterization

Figures 5-a and 5-b show the cyclic voltammograms obtained in the supporting electrolyte (1.0 M NaOH) at a sweep rate of 50 mVs<sup>-1</sup> for both the fresh and heat-treated N1, N2, N3, N4 materials and for the commercial Ni sample. In all cases, a pair of redox peaks (a and b) were observed between 0.280 and 0.625 V vs. Hg/HgO, which are assigned to the Ni<sup>2+</sup>/Ni<sup>+3</sup> pair according to equation 6 [29].





**Figure 5.** Cyclic voltammograms of the fresh and heat-treated N1, N2, N3 and N4 nickel microspheres electrocatalysts. 1.0 M NaOH electrolyte saturated with nitrogen, (5-a and 5-b) in the absence of ethanol at a sweep rate of  $50 \text{ mVs}^{-1}$  and (5-c and 5-d) in the presence of 1.0 M ethanol at  $10 \text{ mVs}^{-1}$ . Peak potentials a, b, c and d.

On the sweep towards positive potentials, the first peak is associated with the oxidation of Ni to  $\text{Ni}^{2+}$ . As the number of potential sweeps increases, the current increases; i.e., there is an increase in electroactive  $\text{Ni}^{2+}$  and  $\text{Ni}^{3+}$  species present on the surface of the electrode. On the return sweep towards negative potentials, a peak (c) is observed at approximately  $-0.3 \text{ V}$  (Fig. 5-a and 5-b) associated with the reduction of  $\text{Ni}^{2+}$  to  $\text{Ni}^0$ . Slight changes in the position of the oxidation and reduction peaks are observed, probably due to the electrochemical synthesis of crystalline nickel hydroxide and nickel oxyhydroxide structures that form a thin film over the surface of the electrode [34]. It has been reported that the electro-oxidation process of Ni electrodes generates the  $\alpha\text{-Ni(OH)}_2$  species, which is slowly converted to the  $\beta\text{-Ni(OH)}_2$  form [35-37].

The electrochemically active surface area (ESA) for Ni electrocatalysts was determined by measuring the Coulombic charge (Q) of the anodic peak corresponding to the region of  $\text{Ni(OH)}_2$  formation, after the double-layer correction. The charge required for the formation of a monolayer of  $\alpha\text{-Ni(OH)}_2$  on the Ni surface has been reported to have a value of  $514 \mu\text{Ccm}^{-2}$  [38, 39]. ESAs were

calculated for all of the Ni electrodes using the equation  $ESA = Q/(0.514(\text{grams of Ni}))$  (Table 3). It is notable that the ESA value drops considerably following heat treatment, mainly due to the formation of  $Ni_3P$ . Additionally, it can clearly be observed that the fresh and treated N3 samples exhibited the greatest catalytically active area. This can be attributed to the increased presence of nickel nanoparticles and the formation of few nickel microspheres (Figs. 1c and 2c). Comparatively, all prepared materials showed higher active areas than the commercial Ni sample (Table 3).

Figures 5-c and 5-d show the CVs of the two series (fresh and heat-treated N1-N4 catalysts) in the working medium of 1.0 M NaOH + 1.0 M  $CH_3CH_2OH$ . The scan rate was  $10 \text{ mVs}^{-1}$ . All of the Ni materials presented catalytic activity for ethanol oxidation. An oxidation peak is observed in the sweep towards positive potentials that begins at approximately 0.430 V (Fig. 5-c and 5-d). Heat treatment has an observable negative effect on catalytic activity (Fig. 5-d). This is attributed to the formation of the  $Ni_3P$  compound, which results in a reduction in the quantity of active sites. This matches the ESA values, which show that the fresh N1-N4 catalysts have a greater catalytically active area for the ethanol oxidation reaction (EOR) than the heat-treated ones (Table 3). On the other hand, a reduction in the current density is observed at the peak maxima of the EOR. This also confirms the reduction of the catalytic area of the electrodes. In both series of N1-N4 catalysts, the cathodic current peaks (b and c) disappear due to the intermediate species generated or ethanol molecules occupying the Ni catalytic sites, i.e., as a result of poisoning the electrode surface during the ethanol electro-oxidation process [29].

Table 3 shows the onset potential values for the ethanol oxidation reaction, the catalytically active area, the main peak potentials and their respective current density or normalized current with respect to ESA for the voltammograms obtained in the absence and presence of 1.0 M EtOH, respectively. For the fresh N1-N4 electrocatalysts, N1 had the lowest onset potential value for the EOR (0.425 V) and the greatest current signal normalized with respect to ESA with a value of  $18.198 \text{ mA}(\text{mgcat})^{-1}$  at 0.710 V. This means that there was a greater quantity of the active form of nickel hydroxide/nickel oxyhydroxide on the electrode surface. This agrees with the fact that it presented the greatest current density in the voltammogram in the absence of ethanol:  $0.398 \text{ mAcm}^{-2}$  for the peak present at 0.491 V. This is probably due to the morphology of the Ni microspheres for the N1 formulation, which are better defined and separated compared to those of N2, N3 and N4 (Fig. 1). The second most catalytically active material was N4, with a current of  $14.394 \text{ mA}(\text{mgcat})^{-1}$  at 0.701 V. However, its onset potential for the EOR was greater at 0.440 V.

For the heat-treated N1-N4 catalysts, the onset potential values were ordered as follows:  $N1 < N4 < N2 < N3$  (Table 3). Similar to the series of fresh materials, the N1 material also presented the greatest current:  $10.847 \text{ mA}(\text{mgcat})^{-1}$  at 0.683 V. However, the non-heat-treated N1 catalyst exhibited the best performance for the electro-oxidation of ethanol in an alkaline medium of the two series (Table 3). All the materials, fresh and heat treated, showed an activity superior to the commercial Ni catalyst.

**Table 3.** EOR-Onset potential, ESA, peak potential and current density values of the N1-N4 electrocatalysts in 1.0 M NaOH (a-c) + 1.0 M CH<sub>3</sub>CH<sub>2</sub>OH (d) at room temperature.

Catalyst	Untreated fresh materials				Heat treated materials			
	EOR-Onset potential (V)	ESA (m <sup>2</sup> gcat <sup>-1</sup> )	Main Peak Potential (V)	Current density j (mAcm <sup>-2</sup> )	EOR-Onset potential (V)	ESA (m <sup>2</sup> gcat <sup>-1</sup> )	Main Peak Potential (V)	Current density j (mAcm <sup>-2</sup> )
N1	0.425	22.8	a: 0.491 b: 0.359 c: -0.380 d: 0.710	0.398 -0.245 -0.161 *18.198	0.427	9.40	a: 0.479 b: 0.371 c: -0.298 d: 0.683	0.467 -0.199 -0.401 *10.847
N2	0.429	26.2	a: 0.483 b: 0.371 c: -0.347 d: 0.762	0.341 -0.152 -0.105 *13.802	0.432	24.5	a: 0.474 b: 0.364 c: -0.304 d: 0.636	0.326 -0.168 -0.087 *7.224
N3	0.445	52.6	a: 0.518 b: 0.416 c: -0.241 d: 0.734	0.364 -0.156 -0.087 *10.774	0.437	36.7	a: 0.499 b: 0.389 c: -0.296 d: 0.669	0.327 -0.131 -0.065 *6.976
N4	0.440	32.0	a: 0.491 b: 0.381 c: -0.309 d: 0.701	0.321 -0.138 -0.114 *14.394	0.430	27.0	a: 0.481 b: 0.364 c: -0.243 d: 0.732	0.396 -0.186 -0.089 *8.673
Commercial Ni Sample	0.431	0.26	a: 0.507 b: 0.342 c: -0.508 d: 0.629	0.206 -0.119 -0.035 3.074	---	---	---	---

d: indicates the main peak potential of ethanol oxidation reaction (EOR) and \*indicates the corresponding electrochemical response normalized with respect to ESA and expressed in mA(mgcat)<sup>-1</sup>.

Figure 6 shows the Nyquist plots of the fresh N1 to N4 electrocatalysts in 1.0 M NaOH + 1.0 M CH<sub>3</sub>CH<sub>2</sub>OH. These were obtained at DC potentials of 0.45, 0.50 and 0.60 V vs. Hg/HgO (taking into account the CVs of Figure 5-c). To analyze the data, the complex nonlinear least squares (CNLS) fitting method was used, and an equivalent circuit was proposed. All of the parameters obtained from the simulation are found in Table 4.

In the impedance spectra in Figs. 6a to 6c, two continuous depressed semi-circles can be observed in the high, medium and low frequency regions. The reaction occurs at 0.45 V. There is probably a mixed process of nickel hydroxide formation and ethanol oxidation at high and medium frequencies, given that the applied potential is more positive than the thermodynamic potential for ethanol oxidation. The low-frequency spectra may be due to the adsorption of intermediates during the oxidation of nickel hydroxide and ethanol [40]. The Nyquist plots at 0.50 and 0.60 V (Figs. 6-b and 6-c) are very similar in shape and trend, except for the diameter of the depressed semi-circles, which are smaller than those at 0.45 V.

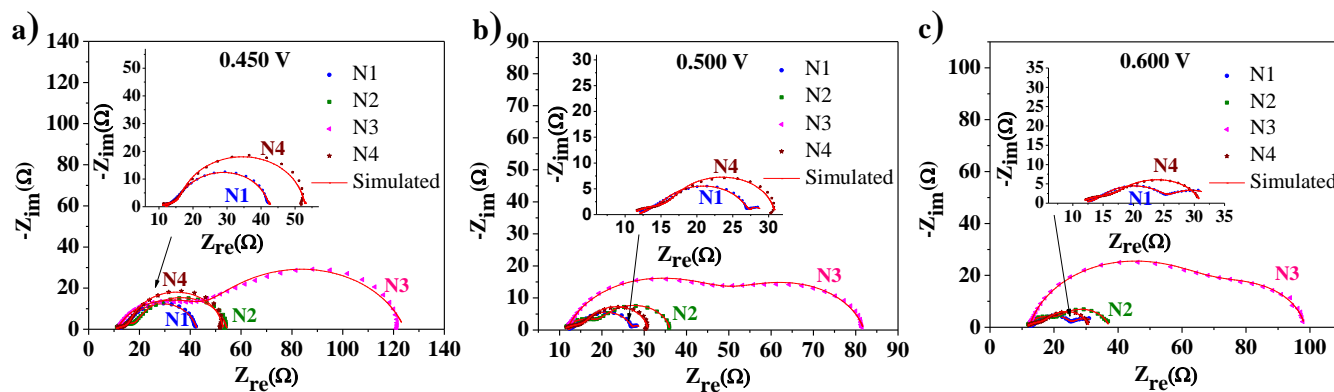


**Figure 6.** Nyquist plots for the ethanol electro-oxidation at the non-heat-treated N1, N2, N3 and N4 electrocatalysts. Electrolyte 1.0 M NaOH + 1.0 M CH<sub>3</sub>CH<sub>2</sub>OH, a) 0.450 V, b) 0.500 V and c) 0.600 V.

The equivalent circuit compatible with the Nyquist plots is presented in Fig. 7. To obtain the impedance simulation for ethanol electro-oxidation, it is necessary to replace capacitor C in the equivalent circuit with a constant phase element (CPE) because the double-layer charge is distributed along the length of the pores on the electrode [41]. In this equivalent circuit, R1, CPE1 and R2, respectively, represent the electrolyte resistance, a constant phase element corresponding to the capacitance of the double-layer and the pores of the electrode, and the charge transfer resistance. CPE2 and R3 are the elements related to the adsorption of intermediates generated in the EOR [29].

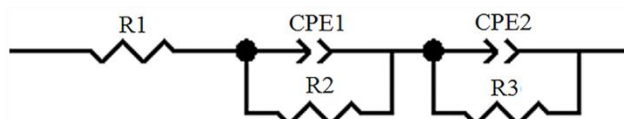


**Figure 7.** Equivalent circuit compatible with the experimental impedance data in Figs. 6-a to 6-c and 8-a to 8-c.

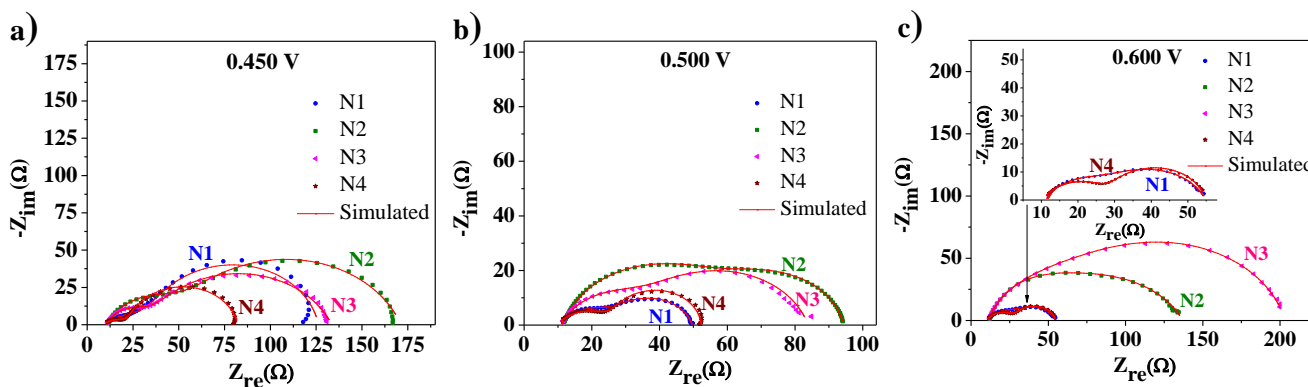
Table 4 contains the parameters of the equivalent circuit of the impedance spectra for ethanol oxidation with the fresh N1 to N4 electrocatalysts. In general, the resistance of the solution has a value close to 11  $\Omega$ . Catalyst N1 exhibited the lowest charge transfer resistance value: 21.9, 8.4 and 8.7  $\Omega$  at DC potentials of 0.45, 0.50 and 0.60 V, respectively. CPE1 has a character ( $N = 0.99$  and  $0.98$ ) close to a capacitor ( $N = 1$ ) at 0.45 and 0.50 V. However, but at 0.60 V ( $N = 0.87$ ), it has a character between a capacitor and a Warburg response ( $N = 0.5$ ). As such, N1 exhibited the lowest resistance for the EOR in an alkaline medium. This matches the cyclic voltammetry study in the presence of ethanol, in which it exhibited the greatest catalytic activity for ethanol oxidation (Table 3).

Figure 8 shows the EIS Nyquist plots for the ethanol electro-oxidation at the same DC potentials chosen for the heat-treated N1 to N4 electrocatalysts in the working medium. Figs. 8-a to 8-c show two continuous semicircles similar to the fresh materials in the high, medium and low frequency regions. The semicircles are due to the charge transfer resistance in the high frequency region and the

adsorption of intermediates in the low frequency regions. The impedance spectra for N1 and N4 are lower than those for N2 and N3 at DC potentials of 0.50 and 0.60 V, respectively. In other words, mass transfer is not affected at these potentials, in contrast with what occurs with the N2 and N3 catalysts, where the impedance is clearly seen to be greater. The experimental data were fitted to the same equivalent circuit model (Fig. 7).

**Table 4.** Equivalent circuit parameters obtained from the simulation of electrical elements for the electro-oxidation of ethanol with the fresh N1-N4 electrocatalysts in the working solution at 0.45, 0.50 and 0.60 V.

$E_{applied}$ (V)	Catalyst	R1 ( $\Omega$ )	CPE1 (F) X $10^{-5}$	N	R2 ( $\Omega$ )	CPE2 (F) X $10^{-4}$	N	R3 ( $\Omega$ )	$\chi^2$ X $10^{-3}$
0.45	N1	11.7	157.0	0.99	21.9	107.0	0.46	9.3	1.41
	N2	10.4	86.0	0.89	35.4	2.7	0.66	8.6	0.95
	N3	11.2	5.6	0.77	34.9	8.4	0.79	78.	1.23
	N4	10.0	99.6	1.0	33.1	102.4	0.33	2 10. 6	1.69
0.50	N1	11.5	140.1	0.98	8.4	171.9	0.37	9.2	1.21
	N2	11.1	54.6	0.94	15.9	1.2	0.74	9.0	0.37
	N3	11.7	3.6	0.81	38.9	6.1	0.85	31.	0.85
	N4	10.5	83.0	1.0	12.4	32.0	0.45	2 8.0	0.77
0.60	N1	11.7	156.6	0.87	8.7	149.8	0.36	5.7	0.19
	N2	11.5	57.3	0.85	16.3	0.67	0.80	9.4	0.48
	N3	12.2	2.0	0.85	59.2	3.6	0.90	27.	0.71
	N4	10.8	96.5	0.92	11.9	20.1	0.47	0 8.4	0.13



**Figure 8.** Nyquist plots for the electro-oxidation of ethanol with the heat-treated N1, N2, N3 and N4 electrocatalysts. Electrolyte 1.0 M NaOH + 1.0 M EtOH, a) 0.450 V, b) 0.500 V and c) 0.600 V.

Table 5 shows the equivalent circuit parameters of the impedance spectra for the electro-oxidation of ethanol with heat-treated N1 to N4 catalysts. The heat-treated N1 catalyst also exhibited the lowest charge transfer resistance value ( $R_2$ ), of 22.6 and 16.2 ohms at potentials of 0.50 and 0.60 V, respectively (Table 5), although not at 0.45 V, where the lowest value was 39.8  $\Omega$  for the N2 material. CPE1 has a character ( $N = 0.84$  and  $0.76$ ) between a capacitor and a Warburg response at 0.50 and 0.60 V, respectively. Heat treatment therefore has a negative effect on charge transfer resistance; i.e., the catalysts have lower activity for the EOR than the fresh electrocatalysts. Nevertheless, N1 also matches the CV results (Table 3).

**Table 5.** Equivalent circuit parameters obtained from the simulation of electrical elements for the electro-oxidation of ethanol at 0.45, 0.50 and 0.60 V with the heat-treated N1-N4 electrocatalysts.

$E_{\text{applied}}$ (V)	Catalyst	$R_1$ ( $\Omega$ )	CPE1 (F) $\times 10^{-5}$	N	$R_2$ ( $\Omega$ )	CPE2 (F) $\times 10^{-4}$	N	$R_3$ ( $\Omega$ )	$\chi^2$ $\times 10^{-3}$
0.45	N1	9.2	96.5	0.91	86.2	11.2	0.48	31.1	2.35
	N2	11.2	7.6	0.80	39.8	7.2	0.78	120	5.41
	N3	10.7	54.1	0.75	99.8	0.4	0.81	22.8	3.06
	N4	8.4	55.4	0.89	58.1	5.8	0.48	15.7	1.51
0.50	N1	10.8	92.6	0.84	22.6	1.6	0.72	16.1	1.17
	N2	11.6	50.2	0.89	34.3	0.4	0.84	48.3	3.96
	N3	11.1	29.6	0.82	47.7	0.5	0.79	25.0	1.37
	N4	9.8	30.3	0.96	25.1	1.3	0.63	17.4	1.88
0.60	N1	11.3	9.5	0.76	16.2	5.9	0.77	27.3	0.97
	N2	11.6	1.7	1.0	29.3	1.6	0.72	96.1	0.86
	N3	11.4	7.6	0.84	140.0	0.3	0.83	52.0	0.28
	N4	10.5	4.4	0.73	18.4	3.6	0.88	25.9	6.67

Table 6 summarizes the catalytic activity for ethanol electrooxidation registered with different Ni based catalysts reported in previous studies [7, 8, 13, 29, 42-47] and in this work. The onset potential exhibited by Ni-based materials is similar, close to 0.6 vs NHE. Meanwhile, for catalysts containing Pt or Pd, the onset potential is lower. Comparing the current density is more difficult since the normalization of the current density with respect to the electroactive area is not done in most of the works cited in Table 6. In this work, we obtained a normalized current density of  $18.12 \text{ mA}(\text{mgcat})^{-1}$ , while Barbosa and colleagues [45] evaluated the oxidation of ethanol with polycrystalline Ni foil; performing the CV test at  $T = 25^\circ \text{C}$  they obtained a normalized current density of  $16.73 \text{ mAcm}^{-2}$ .

**Table 6.** Summary of the catalytic activity for the ethanol electrooxidation in alkaline media using different Ni electrodes. Onset potential and current density values from cyclic voltammetry tests.

Electrocatalyst	Fuel composition	CV conditions	Reference electrode	E Onset (V)	Current density (mAcm <sup>-2</sup> )	Ref.
Ni/Graphite Ni electrodeposition on Graphite rod from 0.05 M NiSO <sub>4</sub> at -1.1 V for 150 s.	1 M CH <sub>3</sub> CH <sub>2</sub> OH + 0.5 M NaOH	From -1 to 1.4 V at 50 mVs <sup>-1</sup> T = 25 °C	Ag/AgCl	0.357	162	[42]
Ni/aHC:activated hydrothermal carbon	1 M CH <sub>3</sub> CH <sub>2</sub> OH + 1M NaOH	From 0.1 to 0.8 V at 50 mVs <sup>-1</sup> , T = 25 °C	Hg/HgO	0.43	28.57	[43]
NiNC (Ni nanorods with N-doped activated carbon)	1 M CH <sub>3</sub> CH <sub>2</sub> OH + 0.1 M NaOH	From 0.0 to 0.7 V, 50 mVs <sup>-1</sup>	SCE	0.346	71.22	[44]
Polycrystalline Ni foil	0.5 M CH <sub>3</sub> CH <sub>2</sub> OH + 1 M NaOH	From 1.125 to 1.58 V at 50 mVs <sup>-1</sup> , T = 25 °C	RHE	1.345	16.73*	[45]
Ni nanospheres	1 M CH <sub>3</sub> CH <sub>2</sub> OH + 1 M NaOH	From -1.0 to 0.8 V at 50 mVs <sup>-1</sup> , T = 25 °C	MMO	0.425	18.12*	This work
Ni nanopowder Commercial sample	1M CH <sub>3</sub> CH <sub>2</sub> OH + 1M NaOH	From -1.0 to 0.8 V at 50 mVs <sup>-1</sup> , T = 25 °C	MMO	0.431	3.074	This work
Ni-B NTs	0.5 M CH <sub>3</sub> CH <sub>2</sub> OH + 0.1 M NaOH	From 0.0 to 0.7 V, 50 mVs <sup>-1</sup>	Ag/AgCl	0.46	19.2	[7]
Ni-Cr <sub>2</sub> O <sub>3</sub> /C	2.0 M CH <sub>3</sub> CH <sub>2</sub> OH + 0.1 M NaOH	From -0.5 to 1.2 V at 50 mVs <sup>-1</sup> , T = 30 °C	MMO	0.50	327	[47]
Ni	0.2 M CH <sub>3</sub> CH <sub>2</sub> OH + 0.1 M KOH	From 0.0 to 0.5 V, 50 mVs <sup>-1</sup> , T = 30 °C	Ag/AgCl	0.34	6.21	[29]
Ni/Pt 60 s Pt deposited on Ni foil	1 M CH <sub>3</sub> CH <sub>2</sub> OH + 1 M NaOH	From -0.9 to 0.43 V, 50 mVs <sup>-1</sup> , T = 25 °C	MMO	-0.58	347.41	[13]
Pd <sub>2</sub> Ni <sub>3</sub> /C	1 M CH <sub>3</sub> CH <sub>2</sub> OH + 1 M KOH	From -0.926 to 0.274 V, 50 mVs <sup>-1</sup>	MMO	-0.65	217	[8]

#### 4. CONCLUSIONS

Nickel microspheres were manufactured via the autocatalytic reduction of NiSO<sub>4</sub>·6H<sub>2</sub>O in a microemulsion at 80 °C. Synthesis conditions in the microemulsion formulation (water-SDS-pentanol) affect the morphology and catalytic activity of the Ni spheres for ethanol electro-oxidation. The sizes of the nickel microspheres based on their average diameters ranged from 0.37 to 1.47 μm. A mixture of metallic nickel and nickel phosphide (Ni<sub>3</sub>P) was obtained by subjecting the materials to heat treatment in nitrogen atmosphere at 300 °C for 4 h. The results revealed that the fresh N1-N4 electrocatalysts presented greater catalytic activity for the EOR in an alkaline medium (1.0 M NaOH) than the heat-treated catalysts. The potentiostatic electrochemical impedances of the fresh and heat-

treated N1 to N4 catalysts for the electro-oxidation of ethanol reaction presented two depressed semi-circles, which indicates that they give rise to two faradaic reactions at the same applied DC potential, i.e., the formation of  $\text{Ni}^{2+}/\text{N}^{3+}$  active species and the oxidation of ethanol. The nickel microspheres with the best performance parameters were N1 and N4, both fresh and heat-treated. The morphology of the particle has a significant effect on catalytic activity for ethanol oxidation. The spherical form could promote mass transfer, either of ethanol or of intermediate species, compared to the materials that were composed of mixtures of Ni spheres and amorphous nanoparticles.

#### ACKNOWLEDGMENTS

The authors acknowledge the financial support received from the projects CONACYT-181106 and SENER-254667. A. Altamirano-Gutiérrez is grateful for the postdoctoral grant. XRD and SEM-EDX measurements were performed at LANNBIO CINVESTAV-Mérida, under support from projects FOMIX-Yucatán 2008-108160 and CONACYT LAB-2009-01 No. 123913. Technical help provided by Dra. Patricia Quintana Owen, M.C. Daniel Aguilar Treviño, M.C. Dora A. Huerta and Q. Ana Ruth Cristóbal is gratefully acknowledged.

#### References

1. Y. Wang, S. Zou, W.B. Cai, *Catal*, 5 (2015) 1507.
2. K. Sundmacher, *Ind. Eng. Chem. Res.*, 49 (2010) 10159.
3. E. Antolini, E.R. Gonzalez, *J. Power Sources*, 195 (2010) 3431.
4. S. Rousseau, C. Coutanceau, C. Lamy, J.M. Léger, *J. Power Sources*, 158 (2006) 18.
5. M.A.A. Rahim, R.M.A. Hameed, M.W. Khalil, *J. Power Sources*, 134 (2004) 160.
6. R.S. Amin, R.M.A. Hameed, K.M. El-Khatib, M.E. Youssef, *Int. J. Hydrogen Energ.*, 39 (2014) 2026.
7. F. Muench, M. Oezaslan, M. Rauber, S. Kaserer, A. Fuchs, E. Mankel, J. Brötz, P. Strasser, C. Roth, W. Ensinger, *J. Power Sources*, 222 (2013) 243.
8. S.Y. Shen, T.S. Zhao, J.B. Xu, Y.S. Li, *J. Power Sources*, 195 (2010) 1001.
9. R.M. Van Effen, D.H. Evans, *J. Electroanal. Chem. Interfacial Electrochem.*, 103 (1979) 383.
10. A.J. Motheo, S.A.S. Machado, F.J.B. Rabelo, J.R. Santos, *J. Braz. Chem. Soc.*, 5 (1994) 161.
11. J. Taraszewska, G. Rosłonek, *J. Electroanal. Chem.*, 364 (1994) 209.
12. M.W. Khalil, M.A.A. Rahim, A. Zimmer, H.B. Hassan, R.M.A. Hameed, *J. Power Sources*, 144 (2005) 35.
13. P. Mukherjee, J. Bagchi, S. Dutta, S.K. Bhattacharya, *Appl. Catal. A-Gen.*, 506 (2015) 220.
14. Y. Wang, W. Chen, D. Pan, Q. Xu, J. Ma, J. Zheng, R. Li, *Int. J. Electrochem. Sci.*, 12 (2017) 2194.
15. M. Ning, H. Zhu, Y. Jia, H. Niu, M. Wu, Q. Chen, *J. Mater. Sci.*, 40 (2005) 4411.
16. X. Lu, G. Liang, Z. Sun, W. Zhang, *Mater. Sci. Eng. B*, 117 (2005) 147.
17. Q. Liu, H. Liu, M. Han, J. Zhu, Y. Liang, Z. Xu, Y. Song, *Adv. Mater.*, 17 (2005) 1995.
18. J. Bao, Y. Liang, Z. Xu, L. Si, *Adv. Mater.*, 15 (2003) 1832.
19. Y. Deng, L. Zhao, L. Liu, B. Shen, W. Hu, *Mater. Res. Bull.*, 40 (2005) 1864.
20. J. Jiang, H. Lu, L. Zhang, N. Xu, *Surf. Coat. Technol.*, 201 (2007) 7174.
21. X. Chen, W. Yang, S. Wang, M. Qiao, S. Yan, K. Fan, H. He, *New J. Chem.*, 29 (2005) 266.
22. M. Fleischmann, K. Korinek, D. Pletcher, *J. Chem. Soc. Perk. Trans. 2*, 0 (1972) 1396.
23. G. Vértes, G. Horányi, *J. Electroanal. Chem. Interfacial Electrochem.*, 52 (1974) 47.
24. J. Ribeiro, F.L.S. Purgato, K.B. Kokoh, J.M. Léger, A.R. De-Andrade, *Electrochim. Acta*, 53 (2008) 7845.
25. F. Vigier, C. Coutanceau, F. Hahn, E.M. Belgsir, C. Lamy, *J. Electroanal. Chem.*, 563 (2004) 81.
26. Z.X. Liang, T.S. Zhao, J.B. Xu, L.D. Zhu, *Electrochim. Acta*, 54 (2009) 2203.

27. C.W. Liu, Y.W. Chang, Y.C. Wei, K.W. Wang, *Electrochim. Acta*, 56 (2011) 2574.
28. F.H.B. Lima, E.R. Gonzalez, *Electrochim. Acta*, 53 (2008) 2963.
29. J.W. Kim, S.M. Park, *J. Korean Electrochem. Soc.*, 8 (2005) 117.
30. S.E. Friberg, C. Brancewicz, D.S. Morrison, *Langmuir*, 10 (1994) 2945.
31. S. Maximovitch, G. Bronoel, *Electrochim. Acta*, 26 (1981) 1331.
32. C. Bernardi, V. Drago, F.L. Bernardo, D. Girardi, A.N. Klein, *J. Mater. Sci.*, 43 (2008) 469.
33. B.D. Cullity, *Elements of X-Ray Diffraction*, Addison-Wesley, (1978) Massachusetts, USA.
34. A.A. El-Shafei, *J. Electroanal. Chem.*, 471 (1999) 89.
35. I. Danaee, M. Jafarian, A. Mirzapoor, F. Gobal, M.G. Mahjani, *Electrochim. Acta*, 55 (2010) 2093.
36. F. Hahn, B. Beden, M.J. Croissant, C. Lamy, *Electrochim. Acta*, 31 (1986) 335.
37. H. Xu, S.L., Y.L. Guo, Y.J. Li, K. C. Shen, C.S. Guan, W.M. Wang, *Int. J. Electrochem. Sci.*, 10 (2015) 4985.
38. S.A.S. Machado, L.A. Avaca, *Electrochim. Acta*, 39 (1994) 1385.
39. I.J. Brown, S. Sotiropoulos, *Electrochim. Acta*, 46 (2001) 2711.
40. X.Z.R. Yuan, C. Song, H. Wang, J. Zhang, *Electrochemical Impedance Spectroscopy in PEM Fuel Cells. Fundamentals and Applications*. Springer, (2010) London, UK.
41. I. Danaee, M. Jafarian, F. Forouzandeh, F. Gobal, M.G. Mahjani, *Int. J. Hydrogen Energ.*, 34 (2009) 859.
42. A.B. Soliman, H.S. Abdel-Samad, S.S. Abdel Rehim, M.A. Ahmed, H.H. Hassan, *J. Power Sources*, 325 (2016) 653.
43. A. Cuña, C. Reyes Plascencia, E.L. Da Silva, J. Marcuzzo, S. Khan, N. Tancredi, M.R. Baldan, C. De Fraga Malfatti, *Appl. Catal. B-Environ.*, 202 (2017) 95.
44. W. Shi, H. Gao, J. Yu, M. Jia, T. Dai, Y. Zhao, J. Xu, G. Li, *Electrochim. Acta*, 220 (2016) 486-492.
45. A.F.B. Barbosa, V.L. Oliveira, J. Van Drunen, G. Tremiliosi-Filho, *J. Electroanal. Chem.*, 746 (2015) 31.
46. H.B. Hassan, Z.A. Hamid, *Int. J. Hydrogen Energ.*, 36 (2011) 5117.

© 2018 The Authors. Published by ESG ([www.electrochemsci.org](http://www.electrochemsci.org)). This article is an open access article distributed under the terms and conditions of the Creative Commons Attribution license (<http://creativecommons.org/licenses/by/4.0/>).